Available online at www.sciencedirect.com
ScienceDirect
Journal of Power Sources 165 (2007) 315–323
JOURNAL OF POWER SOURCES
www.elsevier.com/locate/jpowsour

A picoscale catalyst for hydrogen generation from $NaBH_4$ for fuel cells

R. Peña-Alonso [a,b], A. Sicurelli [a], E. Callone [a], G. Carturan [a], R. Raj [b,*]

[a] *Dipartimento di Ingegneria dei Materiali e Tecnologie Industriali, Università di Trento, Via Mesiano, 77, 38050 Trento, Italy*
[b] *Department of Mechanical Engineering, University of Colorado at Boulder, Boulder, CO 80309-0427, USA*

Received 7 November 2006; received in revised form 18 December 2006; accepted 20 December 2006
Available online 30 December 2006

Abstract

$NaBH_4$, a safe and high energy density source of H_2 for fuel cells, requires a catalyst for reliable hydrogen production. In this paper we show that Pt and Pd atoms, apparently dispersed elementally, on *functionalized* surfaces of carbon nanotubes (CNT) leads to the highest value for the figure of merit ($300\,L\,min^{-1}\,g_{metal}^{-1}\,[NaBH_4]^{-1}$) reported so far in the literature. This result was achieved with a 150 μm thick CNT paper. Thinner paper produces even higher rates of hydrogen generation. The catalyst is robust, continuing to operate without degradation in performance for more than 20 cycles. The kinetic data are analyzed by a combination of first order and zero order reactions. The analysis provides a framework for predicting the performance of the catalyst for fuel cell applications.

Keywords: Catalyst; Hydrogen generation; Sodium borohydride

1. Introduction

Hydride salts such as $NaBH_4$ or $LiBH_4$ constitute safe and practical hydrogen reservoirs for PEM fuel cells. The hydrides are non-toxic, non-inflammable, produce pure hydrogen, and, as shown in Fig. 1, carry a superior weight and volumetric capacity for hydrogen delivery [1]. For these reasons, these hydrides are likely to be the prime candidates as the fuel for cells [2,3] designed for a few watts of electrochemically derived power. However, much larger systems, delivering several kilowatt, are considered feasible with the assumption that the cost of production of $NaBH_4$ will fall with increasing demand [4,5]. While direct-borohydride fuel cells, where the hydride is used directly as the anodic fuel are being developed, the two step, serial configuration where the hydrogen production and its conversion to electric power occurs sequentially appears more feasible for commercial use at the present time [6]. This article is concerned with the hydrogen generation efficiency, control and reliability for the latter design. The figure of merit for such a system is the rate of hydrogen production per gram of the metal catalyst, per molar concentration of $NaBH_4$ ($L\,min^{-1}\,g_{met}^{-1}\,[NaBH_4]^{-1}$; a rate of 1 L min^{-1} at 0.7 V is equivalent to 0.1 kW. Control implies being able to predict the conversion rate from system parameters such as feed rate, power load and temperature. Reliability refers to long-term performance of the catalyst without degradation. These issues remain largely open, primarily because the basic understanding of the kinetics of hydrogen generation from $NaBH_4$ is incomplete.

Catalysts are essential for controlled rate of hydrogen production. On its own $NaBH_4$ reacts exothermally with water [7,8], but the reaction rate diminshes with time as the production of $NaBO_2$ makes the solution alkaline. Controlled production of hydrogen is obtained by buffering the solution at a high pH and then using a catalyst. Nanocrystalline Pt and Ru, supported on various oxide substrates [9–11] have been the most extensively studied. Occasionally free floating clusters of the catalysts, such as Ru [12] and cobalt-boride [13] have also been reported but unsupported catalysts are unlikely to be practical.

The experimental parameters in the study of hydrogen generation are: the yield (expressed as a fraction of the theoretically expected conversion of $NaBH_4$ into hydrogen), the evolution of hydrogen with time as a function of the molar concentration of the aqueous $NaBH_4$ solution, the amount of catalyst used in the reaction, and temperature. The conversion rate is usually expressed in terms of liters of hydrogen generated per minute, per gram of the catalyst. Analytical studies of the kinetics of

* Corresponding author. Tel.: +1 303 492 1029; fax: +1 303 492 3498.
E-mail address: rishi.raj@colorado.edu (R. Raj).

0378-7753/$ – see front matter © 2007 Elsevier B.V. All rights reserved.
doi:10.1016/j.jpowsour.2006.12.043

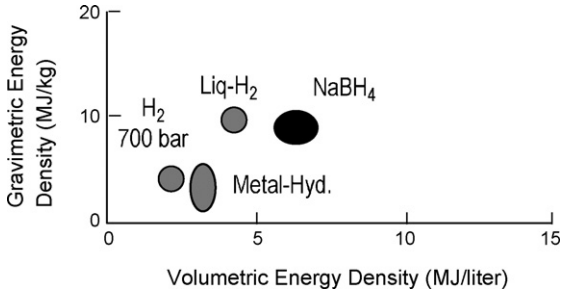

Fig. 1. The gravimetric and volumetric energy density in $NaBH_4$ as compared to other sources of hydrogen. (Data from: Brenstoffzellen-Fahrzeuge von GM/Opel Technik und Markteinfuehrung, Dr. G. Arnold, January 22–23, 2003).

conversion are limited [10,11]. One study considers Pt nanoclusters dispersed on $LiCoO_2$ substrate [10]; the other to a suspension of Ru nanoclusters [11]. Both report zero order kinetics, that is, the rate of hydrogen production is independent of the molar concentration of $NaBH_4$. These results, however, must be considered as being preliminary since the reactions were not studied over a wide range of $NaBH_4$ concentrations. Therefore, the study of the activity of various catalysts remains somewhat disconnected, making it difficult to draw clear conclusions about the choice of the best catalyst for predictable and reliable service in a fuel cell. At the present time the key observations are: the production rate of hydrogen ranges from 0.2 to 2.8 L min^{-1} g_{met}^{-1} [14], the kinetics of the reaction is zero order (although a careful reading often shows the hydrogen production rate to depend on the molar concentration of sodium borohydride), and that the chemistry of the catalyst, and its support, influence its performance.

The catalysis of $NaBH_4$ occurs at the surface of the metal clusters [15]. Therefore the reaction rate increases with a higher surface to volume ratio of the metal clusters [8,16–20]. The "geometric catalytic efficiency" of the metal cluster can be expressed as the ratio of the atoms residing on the surface of the cluster divided by the total number of atoms in the cluster. We call this fraction, n_s; it will be inversely proportional to the radius of curvature, r, of the cluster, since it is dimensionally related to the surface to volume ratio of a spherical shape. Additionally, as shown schematically in Fig. 2, n_s will also be related to the contact angle, θ, formed by the cluster with the substrate. We draw upon the derivations for the surface area and the volume of voids of a lenticular shape at grain boundaries in solids, to obtain an explicit expression for the surface to volume ratio for

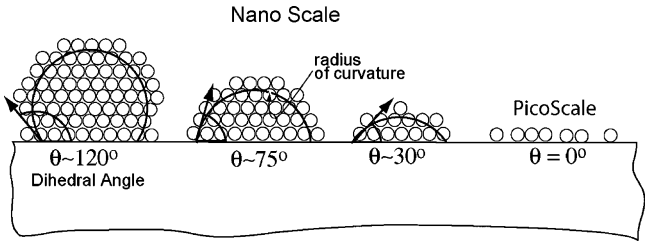

Fig. 2. The influence of contact angle on the surface to volume ratio of the cluster. Elemental, or picoscale dispersion of the metal atoms can be obtained if the contact angle approaches zero.

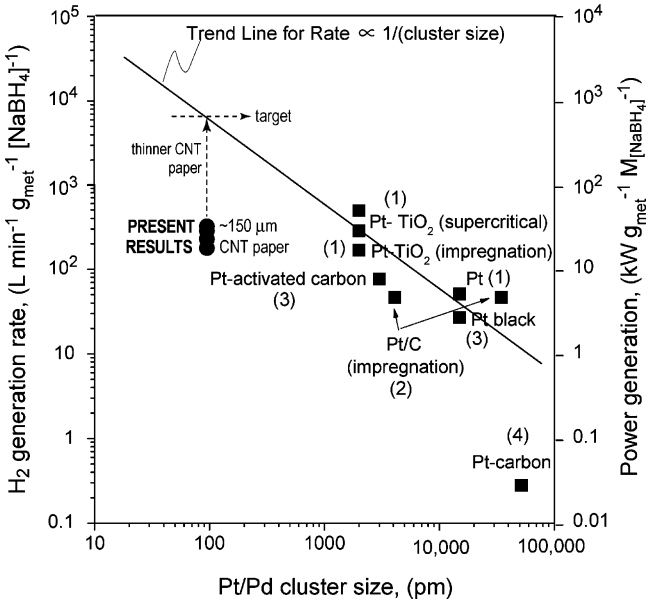

Fig. 3. A plot of the figure of merit for the catalyst as a function of the cluster size of the metal atoms. The trend line is predicted by Eq. (1). The present work is expected to reach the target given by the trend line with thinner specimens of the carbon nanotube paper. (1) Kojima et al. [9], (2) Wu et al. [20], (3) Waco Pure Chemical Industries Ltd., (from Kojima et al. [9]), and (4) Kishida Chem. Co., Ltd. (from Kojima et al. [9]).

the cluster. The volume of the cluster of a spherical segment, as shown in Fig. 2, is given by $r^3(\pi/3)(2-3\cos\theta+\cos^3\theta)$ while its surface area is given by $r^2 2\pi\,(1-\cos\theta)$ [21]. Therefore, the surface to volume ratio of the cluster is given by $H(\theta)/r$, where:

$$H(\theta) = \frac{6(1-\cos\theta)}{2-3\cos\theta+\cos^3\theta} \tag{1}$$

The number of atoms in the volume of the cluster is equal to the volume divided by the effective volume per atom of the metal, which is written as Ω. Similarly, the number of atoms on the surface is equal to the surface area divided by $\Omega^{2/3}$. Therefore the ratio, n_s, is also proportional to $\Omega^{1/3}$. Combining this result with the r dependence of the surface to volume ratio leads to the following equation:

$$n_s = \frac{\Omega^{1/3}}{r} H(\theta) \tag{2}$$

The influence of θ on n_s can be immediately seen from the schematic in Fig. 2. This dependence is given explicitly by the function $H(\theta)$, for example for $\theta = 90°$, $60°$, $30°$, $15°$, and $5°$, $H(\theta) = 3.0$, 4.8, 15.6, 132 and 526, respectively, that is, the surface to volume ratio increases rapidly with a reduction in the contact angle. In the limiting case when $\theta \to 0$, both r and $H(\theta) \to \infty$, and the ratio $n_s \to 1$, its highest possible value.

According to Eq. (2) the catalytic performance should scale inversely as the cluster radius. A comprehensive review of the literature leads to the plot shown in Fig. 3, which gives the hydrogen generation rate from $NaBH_4$ as a function of cluster size. This log–log plot shows the trend line predicted by Eq. (2) with a slope of minus one. The scatter in the data is significant, but

a definite trend towards a higher figure of merit (expressed as $L\,min^{-1}\,g_{met}^{-1}[NaBH_4]^{-1}$) with the decrease of the cluster size is evident.

In this article we present results from experiments with a three tier catalyst constructed from carbon nanotubes, covered with a monolayer of a silicon carbonitride material, which is further coated with a subatomic layer of mixed Pt and Pd atoms. The kinetics of hydrogen generation from alkaline $NaBH_4$ is shown to be predominantly first order. The performance of the catalyst remains robust and reproducible after multiple cycles.

2. Experimental method

2.1. Catalyst preparation

The catalyst architecture was as follows. First a carbon nanotube paper was coated with a monolayer of silicon carbonitride compound by a polymer process, as described in [22]. The carbon nanotubes (CNT) were purchased from Carbon Nanotechnologies Inc., Houston, TX. The same Ref. [22] gives data on the supercapacitance measurements of carbon nanotubes, with and without the silicon carbonitride coating. The measurement of high supercapacitance is evidence that the SiCN coating is electronically conducting. Indeed the supercapacitance of the carbon nanotubes appeared to be somewhat enhanced by the deposition of silicon carbonitride. Experiments on self-standing structures of silicon carbonitride have been shown to be electronically conducting, as well [23].

A submonolayer coating of mixed Pt and Pd atoms was chemically deposited on the functionalized carbon nanotube paper with bis-allyl pentane solutions according to the method reported by O'Brien et al. [24]. Bis-allyl Pt or Pd species are expected to become anchored to reactive support sites [25] facilitating a molecular dispersion. The molecular species are then converted to metal atoms by H_2 reduction. High dispersion of Pd/Pt catalysts prepared in this way has been demonstrated in [26].

To deposit the metal, small pieces of the CNT paper were immersed in the pentane solutions under N_2 at room temperature. The metal concentrations in the solution were $Pt/Pd = 0.06/0.14\,g\,L^{-1}$. After 1 h, the solution was completely removed and the samples were maintained under H_2 flow for 2 h. The samples, now ready for catalytic study, were stored in air. Elemental analysis of Pd and Pt content was obtained by Inductively Coupled Plasma ICP-OES Ciros (Spectro, Germany) at $\lambda_{Pt} = 214.423$ nm and $\lambda_{Pd} = 340.458$ nm. Fragments of the catalyst were dissolved in known volumes of concentrated HCl/HNO_3 3/1 (v/v) and analyzed by ICP-OES. This analysis gave values of 0.42 wt.% Pt and 0.98 wt.% Pd. The relative atomic percentages of Si, Pt and Pd atoms at and near the surface as measured by the energy dispersive X-ray method in a scanning electron microscope (EDS-SEM), gave Pt/Si ratio of 0.10 and Pd/Si ratio of 0.30.

The clustering of Pt and Pd into nanocrystals was investigated by X-ray diffraction. The X-ray diffraction spectra showed completely amorphous structure, implying that Pt/Pd were *not* clustered into nanocrystals. This result strongly suggests that Pt/Pd were elementally distributed on the surface of the carbon nanotubes, especially since previous studies have shown that Pt clusters into nanocrystals, which give rise to Bragg peaks in X-ray diffraction, on "clean" carbon nanotubes [27–32] It should be kept in mind that there are no direct methods for imaging elemental Pt and Pd on the catalyst surface. Quantitative spectroscopic methods such as XPS, using standards as calibration, could provide this information. But such experiments are outside the scope of this paper.

In the present study, the Si atoms in the silicon carbonitride layer, used to functionalize the carbon nanotubes, are suspected to have played a role in achieving an atomic dispersion of the metal atoms. It is known that Pt and Si react to form silicides, suggesting strong bonding between Si and Pt atoms. This strong bonding will impede surface diffusion of the metal atoms that is needed for the growth of clusters.

The specific surface area of the catalyst was measured by N_2-physisorption with a Micromeritics ASAP 2010 Instrument. Samples were degassed below 0.3 Pa at room temperature for several hours before the measurement. The measurements were carried out at the boiling point of liquid nitrogen (∼77 K). The BET equation [33] was used to determine the specific surface area; the BJH method [34] was applied to the adsorption data for determining pore size distributions. The specific surface area of the CNT paper, without the metal deposition, was in the range between 400 and 620 $m^2\,g^{-1}$. With Pt/Pd the specific surface area dropped to 250–350 $m^2\,g^{-1}$ (a reason for this drop in surface area is discussed below). Assuming Pt and Pd to be atomically dispersed it is possible to estimate the fraction of the monolayer of Pt/Pd on the surface of the catalyst. Considering a surface area of 300 $m^2\,g^{-1}$ and taking the atomic radii of Pt and Pd to be 135 and 140 pm, respectively, gives an estimate of 0.0034 of a monolayer of Pt and Pd atoms on the surface, that is, one out of very 300 possible sites on the surface was occupied by a metal atom.

The nitrogen adsorption data as a function of pressure (at liquid nitrogen temperature) are given in the upper graph in Fig. 4. The pore size data derived from this graph are shown in the lower plot. The principal difference between the surface areas, with and without the metal coating, lies in the volume occupied at low pressures where the pore size is in the range of 1–2 nm. Keeping in mind that the nanotube paper was constructed from single wall carbon nanotubes, we propose that the nearly two-fold drop in the surface area is related to the blocking of the open ends of the carbon nanotubes by the Pt/Pd coating process. The blocking means that the inside of the carbon nanotube surfaces cannot be accessed by the nitrogen molecules, which would lead to a drop in the measured surface area by a factor of about two. The radius of the carbon nanotubes is in the 1–2 nm range, which coincides with the range of pore size that accounts for the difference in the surface area of the coated and uncoated carbon nanotubes. We cannot say whether the capping of the end faces of the carbon nanotubes was caused by the Pt/Pd atoms or by the organic bis-allyl (Pt, Pd) oligmers. The latter explanation appears more likely since the organics should bind tightly to the defect sites in the carbon structure present at the end faces of the nanotubes, and, therefore, may have resisted reduction into elemental Pt/Pd by hydrogen.

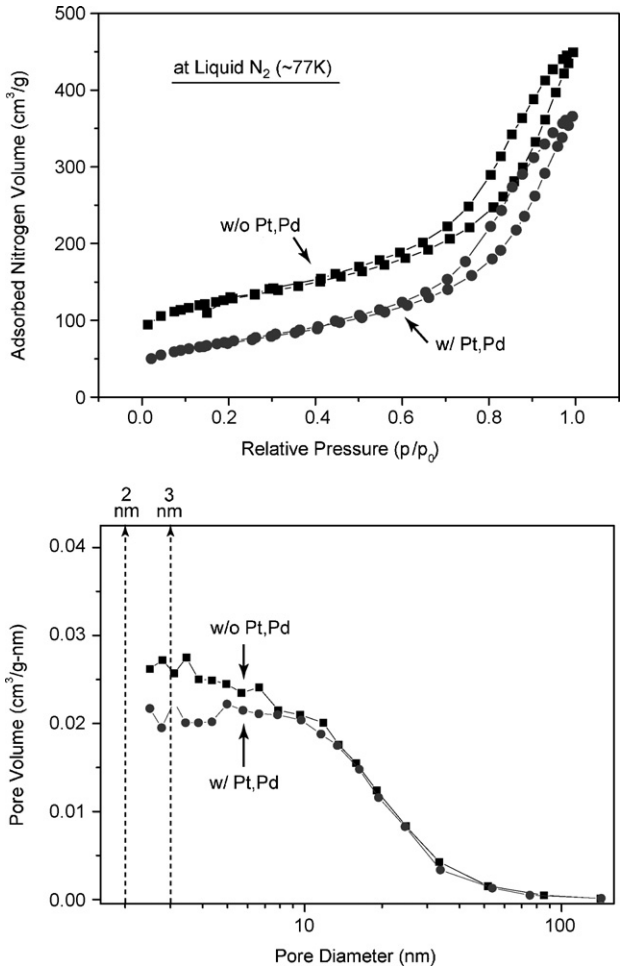

Fig. 4. Nitrogen adsorption/desorption isotherms and pore size distribution according to the BJH method for uncoated and metal coated substrates of carbon nanotubes functionalized with silicon carbonitride.

2.2. Measurements of hydrogen generation

The volume of hydrogen produced was measured as a function of time, using a gas burette connected to the reaction flask. Both the reactor and the burette were thermostated by a water circulating apparatus. The experiments were carried out at ambient pressure in Boulder, CO, which lies in the range 760 ± 8 mm $\times$ 0.854. The sodium borohydride solution was stirred with a magnetic spin bar at 800 rpm to promote interface-controlled reaction between the solution and the catalyst. All experiments were carried out with an amount of $NaBH_4$ solution that would have a theoretical yield of 18 ml of hydrogen at NTP. Four solution concentrations of $NaBH_4$, 0.03, 0.02, 0.015 and 0.01 M, were prepared. The solutions were buffered at pH 13 with KCl/NaOH. Fresh solutions were prepared immediately before every hydrogen generation experiment. In all experiments the theoretically predicted conversion of $NaBH_4$ into hydrogen was achieved. The experiments with the four molar concentrations were carried out at 29 °C. Additionally, experiments were done at 40, 50, and 59 °C at 0.03 M in order to determine the activation energy for the catalytic reaction. All experiments were done with the same catalyst, which had a total

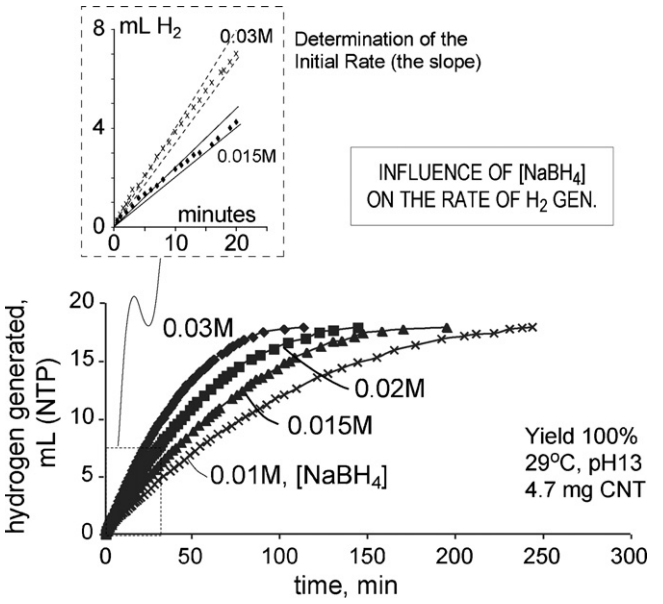

Fig. 5. Hydrogen production as a function of time for four molar concentrations of $NaBH_4$ at 29 °C and pH 13.

weight of 4.1–4.7 mg. The performance of this catalyst remained unchanged even after the same catalyst had been used in 20 experimental runs.

The two sets of results are shown in Figs. 5 and 6. The first gives the hydrogen generation profile for the sets of experiments at 29 °C carried out at four molar concentrations of $NaBH_4$; the second shows the data obtained for the 0.03 M $NaBH_4$ solution at four temperatures. The inset in Fig. 5 shows the procedure for determining the initial rate of hydrogen generation. The average slopes of hydrogen generated versus time for the first 20 min of the data were used to obtain a value for these initial rates. The data in Fig. 5 show that hydrogen generation depends on the molar concentration of sodium borohydride, typical of a non-zero order kinetic behavior.

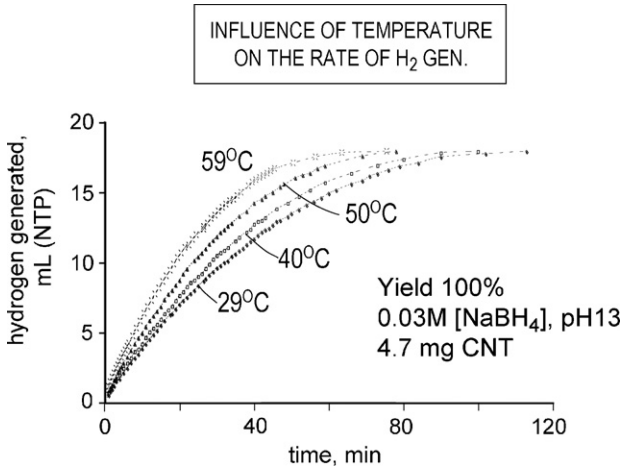

Fig. 6. Hydrogen production at four different temperatures with a 0.03 M $NaBH_4$ solution.

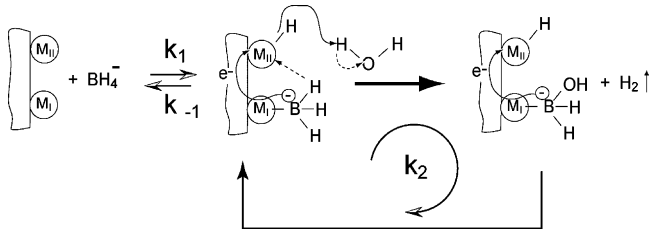

Fig. 7. The proposed mechanism for the catalytic production of H_2 from an aqueous solution of $NaBH_4$.

3. Analysis

The data are analyzed in terms of the mechanism illustrated in Fig. 7. It involves two essential kinetic steps. In the first step the BH_4^- ions in the solution are chemisorbed to the metal atoms. The forward rate of the process is described by the kinetic rate constant k_1, and the backward rate, which is the desorption rate of the ions back into the solution, by k_{-1}. The rate constants are defined by equations such as the one given below for the forward reaction:

$$\left[\frac{\mathrm{d}[\mathrm{MBH_4^-}]}{\mathrm{d}t}\right]_{\text{forward}} = k_1[\mathrm{BH_4^-}][\mathrm{M}] \tag{3}$$

where $[MBH_4^-]$ is equal to metal sites that are *occupied*, [M] is the molar concentration of metal sites that remain *unoccupied*, and $[BH_4^-]$ is the molar concentration of the ions in the solution. Note that the reaction rate is proportional to the first power of [M], because the primary reaction occurs between the unoccupied metal sites and BH_4^- ions. The signficance of the second metal atom which aids the kinetic pathway, as illustrated in Fig. 7, is expressed via the rate constant k_1. However, k_1 will become sensitive to [M] only if the metal atom concentration is so lean that the catalytic reaction becomes limited by the probability of finding a vacant metal site adjacent to the M–BH_4^- site, which in most instances is unlikely since the concentration of metal atoms on the catalyst surface will usually be high.

In the second step the negative charge on the BH_4^- ion is transferred with one hydrogen atom, via the CNT-PDC structure to the adjacent metal atom [35]. The electronic conductivity of the CNT/PDC support is important in such electron transfer [22]. It is possible that the different electron chemical potential of the Pt and Pd atoms facilitates this process. This feature may improve the catalytic performance since the M_I–M_{II}–BH_3 configuration is suitable for OH^- substitution at the B atom. In organometallic metal-alkyl complexes the reconstruction of $HOBH_3^-$ anion is invoked as an alternative to BH_3 dissociation, with the assumption that BH_4^- and $(HO)_nBH_{4-n}^-$ are equally reactive at the catalytic site.

Next, the charged hydrogen atom reacts with a water molecule to produce H_2 and an OH^- which reacts with boron to produce the $BH_3(OH)^-$ ion [36]. The cycle of charge transfer continues as $BH_3(OH)^- \rightarrow BH_2(OH)_2^- \rightarrow BH(OH)_3^- \rightarrow B(OH)_4^-$, releasing molecular hydrogen at each step. Finally the $B(OH)_4^-$ reacts with Na^+ to produce $NaBO_2$. The rate constant for this second cycle, that is the conversion of the metal borohydride complex, MBH_4^-, into hydrogen and $B(OH)_4^-$, is written as k_2. The entire reaction can now be summarized in the following way:

$$\mathrm{M} + \mathrm{BH_4^-} \underset{k_{-1}}{\overset{k_1}{\rightleftarrows}} \mathrm{MBH_4^-} \xrightarrow[k_2]{4\mathrm{H_2O}} \mathrm{M} + 4\mathrm{H_2}\uparrow + \mathrm{B(OH)_4^-} \tag{4}$$

The reaction in Eq. (4) is analyzed in Appendix I and leads to the following result:

$$\frac{1}{v} = \frac{1}{k'}\frac{1}{[\mathrm{NaBH_4}][\mathrm{M}]_0} + \frac{1}{k_2}\frac{1}{[\mathrm{M}]_0} \tag{5}$$

where $[M]_0$ is the molar concentration of the *maximum* number of metal sites available in the solution for the reaction, and $[NaBH_4]$ is the molar concentration of the sodium borohydride remaining in the solution at any time. The derivation of Eq. (5) assumes that sodium borohydride is fully ionized in the aqueous solution. In Eq. (5), v is the rate of consumption of sodium borohydride:

$$v = -\frac{\mathrm{d}[\mathrm{NaBH_4}]}{\mathrm{d}t} \tag{6}$$

In Eq. (5), k', which represents the phenomenological first order rate constant, is given by:

$$k' = \frac{k_1 k_2}{k_2 + k_{-1}} \tag{7}$$

The result in Eq. (7) shows that the first order rate constant, k', is a complex quantity depending on three rate constants, k_1, k_{-1}, and k_2. The equation has two limits: if $k_2 \gg k_{-1}$, then $k' \rightarrow k_1$, but if $k_2 \ll k_{-1}$, then $k' \rightarrow k_1 k_2/k_{-1}$.

Experiments that measure hydrogen generation are usually carried out with parameters that are related to, but are not explicitly the same as those in Eq. (5). In a typical experiment, the hydrogen generated is measured in L min^{-1} from a solution of a prescribed molar concentration of $NaBH_4$, with a certain amount of the metal catalyst, usually reported in grams. Therefore, we define a new set of parameters that can be more easily related to experiments:

$[NaBH_4]$ molar concentration of $NaBH_4$ in the solution (in mol L^{-1}); n_{H_2} moles of hydrogen generated from the solution of sodium borohydride; MW_{met} average molecular weight of the metal species; V volume of the solution (in L); g_{met} total metal content in grams in the solution; K_1 experimental first order rate constant in units of mol H_2 $\mathrm{min}^{-1}\mathrm{g}_{\mathrm{met}}^{-1}[\mathrm{NaBH_4}]^{-1}$; K_2 experimental zero order rate constant in units of mol H_2 $\mathrm{min}^{-1}\mathrm{g}_{\mathrm{met}}^{-1}$.

Since one mole of $NaBH_4$ produces four moles of H_2 we have that:

$$\frac{\mathrm{d}n_{\mathrm{H_2}}}{\mathrm{d}t} = -4V\frac{\mathrm{d}[\mathrm{NaBH_4}]}{\mathrm{d}t} \tag{8}$$

Also,

$$[\mathrm{M}]_0 = \frac{g_{\mathrm{met}}}{\mathrm{MW_{met}}V} \tag{9}$$

Substituting Eqs. (8) and (9) into Eqs. (5) and (6) we obtain:

$$\frac{1}{(\mathrm{d}n_{\mathrm{H_2}}/\mathrm{d}t)} = \frac{1}{K_1}\frac{1}{[\mathrm{NaBH_4}]g_{\mathrm{met}}} + \frac{1}{K_2}\frac{1}{g_{\mathrm{met}}} \tag{10}$$

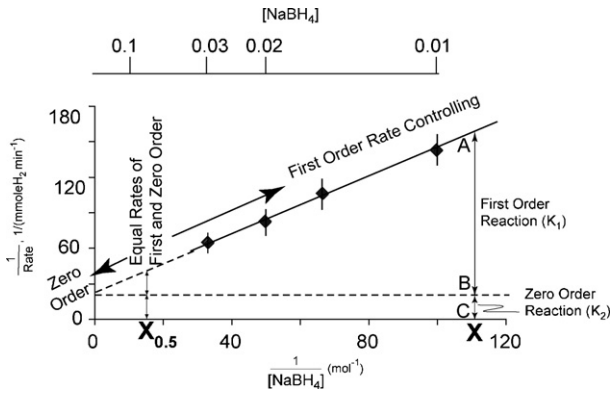

Fig. 8. A kinetic plot of H_2 release data from Fig. 4 according to the prediction from Eq. (10).

where,

$$K_1 = \frac{4k'}{\mathrm{MW_{met}}} \quad \text{and} \quad K_2 = \frac{4k_2}{\mathrm{MW_{met}}} \tag{11}$$

The comparison of the experimental data with Eq. (10), will yield the phenomenological first order and zero order rate constants, K_1 and K_2. The process is to plot the inverse of the initial hydrogen generation rate against the inverse of the initial value of [$NaBH_4$]. The results should fit a straight line. The slope of the line yields a value for K_1, while the intercept of the line for the limit $(1/[NaBH_4]) \rightarrow 0$ gives K_2. (The referees have pointed out that a recent paper published on-line [37] discusses combined zero and first order kinetics in a Ru-on-carbon catalyst. However, while they distinguish between zero and first order in terms of temperature, in the present work the molar concentration of sodium borohydride forms the basis for distinguishing between these two mechanisms).

The above plot for the present data is given in Fig. 8. A good straight line fit, as predicted by Eq. (10) is obtained. The intercept and the slope of the line lead to the following values for the rate constants: $K_1 = 12.9\,\mathrm{mol\,H_2}\,min^{-1}\,\mathrm{g_{met}^{-1}}[NaBH_4]^{-1}$, and $K_2 = 0.7\,\mathrm{mol\,H_2\,min^{-1}g_{met}^{-1}}$.

The graph in Fig. 8 provides an insight into the relative contribution of first order and zero order reactions in hydrogen generation. For example, at the point denoted by X along the horizontal axis the fraction of hydrogen generated by the first order reaction is given by the ratio AB/AC. The remaining fraction, given by BC/AC is the contribution from the zero order reaction. This relationship changes with concentration. At concentration $X_{0.5}$, for example, the two types of reactions make an equal contribution. If $X < X_{0.5}$ then the zero order reaction is dominant, and the first order is more important if $X > X_{0.5}$. In the present experiments the first order reaction played the dominant role, since the concentrations were in the $X > X_{0.5}$ regime.

With the above analysis it is possible to estimate the activation energy for the hydrogen generation process, by writing the rate constant $\propto \exp(-Q/RT)$. A simple Arrehenius plot of the results, where the logarithm of the rate, millilitres of H_2 (at NTP) generated in 20 min, is plotted against inverse temperature, is given in Fig. 9. The point at 29 °C is obtained by considering only the first order component of the reaction rate from the plot in Fig. 8. A good linear fit, with an activation energy of 19 kJ mol^{-1} is obtained. This activation energy is presumed to apply to the first order rate constant. In comparison Amendola et al. [38] in their experiments at high $NaBH_4$ and low NaOH concentration, obtained 56 kJ mol^{-1}. Hua et al. [39] who measured hydrogen generation with a Ni_xB catalyst obtained an activation energy of 38 kJ mol^{-1}. The lower value for the activation energy in the present experiments reflects the specificity of the Pt/Pd-Si catalytic sites.

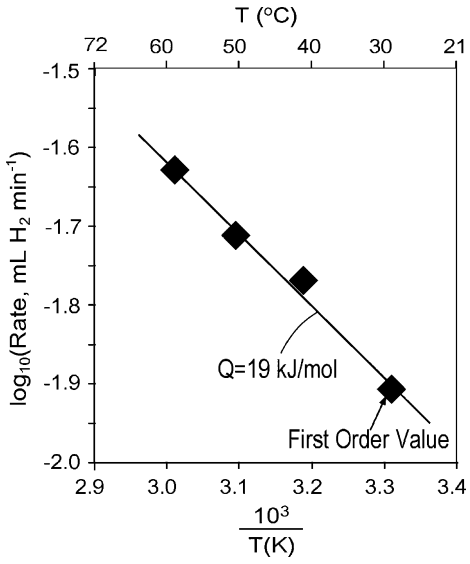

Fig. 9. Arrhenius plot for the determination of the activation energy for the rate constant.

4. Discussion

The work in this article addresses the three issues that are important for a successful application of $NaBH_4$ as the source of hydrogen for fuel cells: the scientific understanding of the reaction kinetics of hydrogen generation, the picoscale chemical design of the catalyst, and the reliability of the catalyst.

The figure of merit (FOM) for the performance of a catalyst is usually expressed as the rate of hydrogen production per unit weight of the precious metal, per molar concentration of the solution. If the metal atoms are clustered together then the efficiency is reduced because only the atoms residing on the surface of the cluster contribute to the reaction. Therefore, the FOM depends both on the cluster size and on the contact angle formed with the supporting substrate. Eqs. (1) and (2) provide a mechanism for quantitatively including this effect in the figure of merit. For example if the total concentration of the metal atoms in the catalyst is given by $[M]_0$ then the effective metal concentration, that is actually involved in the catalytic process, will be given by:

$$[M]_0^{\mathrm{eff}} = [M]_0 n_s = \frac{[M]_0 \Omega^{1/3} H(\theta)}{r} \tag{12}$$

where n_s is the fraction of the atoms in the cluster that are present on the surface of the cluster. Note that n_s becomes smaller for

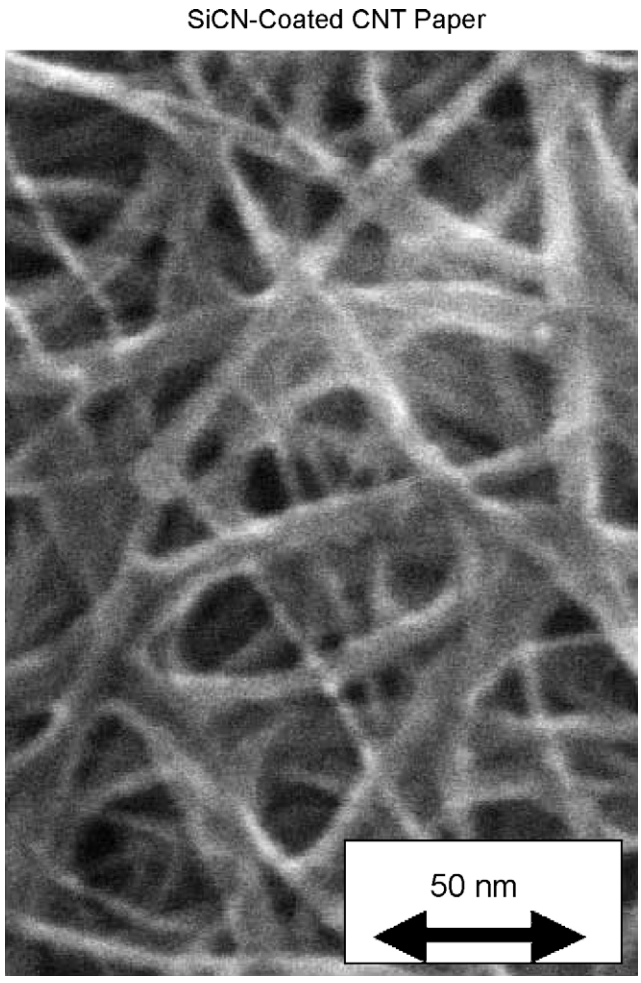

Fig. 10. A scanning electron micrograph of the CNT paper used as the substrate in the present study.

larger particle size and higher contact angles. The upper bound value, when $n_s = 1$ applies only when the metal atoms are distributed as a monolayer or a submonolayer on the surface of the catalyst, as shown on the right in Fig. 2.

The values for FOM from the literature are compared with the present work in Fig. 3. The carbon nanotube paper that formed the basis of the architecture of the present catalyst was 150 μm thick. The typical intertube spacing between the nanotube bundles in the paper, as shown in Fig. 10, was approximately 20 nm. The release of hydrogen from the catalyst is a multistep process. In addition to catalysis, the hydrogen molecules must coalesce into bubbles. The bubbles must then release into the solution. The release of the bubble from the catalyst is a step that is often overlooked. The bubble forms a contact angle with the catalyst surface, which means that it is pinned to the surface requiring a critical buoyancy force before it breaks free. In our experiments the fine CNT mesh places a hindrance to bubble-escape; indeed under a microscope we could not see any bubbles emanating from the interior of the carbon nanotube paper. The implication of this observation is that a thinner paper would increase hydrogen generation on a per gram metal basis. Early experiments with 50 μm paper, instead of the 150 μm paper, have shown about a three-fold increase in rate of hydrogen generation. Our goal is to create a catalyst of a thin CNT paper, just a few micrometers thick, which is expected to produce a 10 to 50 fold increase in the hydrogen production rate from the present level. Interestingly, such a development would meet the target that is predicted from the trend line in Fig. 3.

The catalyst described in this article has a unique architecture. The CNT surfaces are coated with a monolayer of a silicon carbonitride ceramic deposited by a liquid polymer-precursor process. This coating enhances the electrical and electrochemical functional properties of CNT [22]. Studies of Pt deposited directly on to "clean" CNTs has shown that it forms clusters. With the silicon carbonitride interlayer the Pt and Pd atoms remain elementally dispersed. It would seem that the Pt–Si bond plays a key role in this monolayer dispersion. The combination of Pt/Pd catalyst used in the present experiments is also significant. In early experiments, specimens from Pt (only), Pd (only) and the Pt/Pd alloy were prepared. The Pt/Pd combination performed much better than the Pt or the Pd on its own.

The understanding of the kinetics of hydrogen generation is important for prediction of its performance in a fuel cell. The result given in Eq. (5) provides a way of assessing the relative importance of the first order and second order kinetics (the slower one is rate controlling). The data from the present work shows that first order plays a dominant role. The results in the literature are unclear on this issue. It is generally stated that metals on oxides show a zero order kinetics, but a careful examination of the data often shows that first order kinetics is also a contributing factor, as discussed in a recent paper [37]. The methodology presented here can help to clarify the relative contribution from zero and first order kinetics in hydrogen generation experiments.

5. Conclusions

A new catalyst for generating hydrogen from buffered solutions of sodium borohydride has been presented. This high surface area catalyst is made from carbon nanotube paper. The paper is first functionalized with a monolayer of a polymer derived silicon carbonitride ceramic. An elemental dispersion of Pt and Pd, amounting to 0.0034 of a monolayer, is chemically deposited on the functionalized surface of the CNT paper. This catalyst is capable of generating hydrogen at the rate of $300\,\mathrm{min}^{-1}\mathrm{g}_{\mathrm{metal}}^{-1}[\mathrm{NaBH_4}]^{-1}$, which is in the range of the highest value reported so far in the literature. The catalyst is robust, showing negligible degradation even after more than twenty experimental cycles. The CNT paper can be cut and easily handled as needed in fuel cell applications. The performance of the current architecture is limited by the trapping of hydrogen bubbles in the nanotube mesh within the interior of the paper. A thin CNT structure is being developed, which is expected to produce a ten to one to fifty fold increase in performance.

The application of a catalyst in a fuel cell requires predictable performance. For this purpose it is necessary to have knowledge of the nature of the reaction kinetics. A methodology for analyzing kinetic data to distinguish between first order and zero order kinetics is presented. In the present work hydrogen generation

was predominantly controlled by the first order rate constant, with a minor contribution from zero order kinetics.

Acknowledgements

This research was supported by a grant from the Department of Energy, NETL, Morgantown, W. Va., No: DE-FC26-03NT4196, which is gratefully acknowledge. Raquel Peña-Alonso wishes to thank the Ministerio de Educación y Ciencia from Spain for finantial support in the form of a National Fellowship. Shelley Arreguin's results on higher generation rates from thin CNT paper are gratefully acknowledged.

Appendix A

A.1. Derivation of Eq. (5)

The reaction described by Eq. (4) leads to the following two equations, one for the rate of consumption of the borohydride ion, and the other for the rate of change of the concentration of the metal borohydride complex. Under quasi-steady state conditions the concentration of the borohydride complex can be assumed to be constant, and therefore, the second equation is equated to zero. Thus, we have that:

$$v = -\frac{\mathrm{d}[\mathrm{BH_4}^-]}{\mathrm{d}t} = k_2[\mathrm{MBH_4}^-] \tag{A1}$$

and,

$$\frac{\mathrm{d}[\mathrm{MBH_4}^-]}{\mathrm{d}t} = 0$$

$$= k_1[\mathrm{BH_4}^-][\mathrm{M}] - k_{-1}[\mathrm{MBH_4}^-] - k_2[\mathrm{MBH_4}^-] \tag{A2}$$

Now, the unoccupied metal sites are related to the maximum number of sites and the concentration of the metal borohyride complex by:

$$[\mathrm{M}] = [\mathrm{M}]_0 - [\mathrm{MBH_4}^-] \tag{A3}$$

Substituting [M] from (A3) into (A2) gives the following result for $[\mathrm{MBH_4}^-]$:

$$[\mathrm{MBH_4}^{-1}] = \frac{k_1[\mathrm{BH_4}^-][\mathrm{M}]_0}{k_2 + k_{-1} + k_1[\mathrm{BH_4}^-]} \tag{A4}$$

Then, substituting (A4) into the right hand side of (A1) and recognizing that $[\mathrm{BH_4}^-] = [\mathrm{NaBH_4}]$ gives the final result quoted in Eq. (5).

The constants and the values used for various calculations in the text were as follows: (i) Millilitres of H_2 generated in the experiments were converted into to NTP millilitres (at 273 K and 101 Pa pressure) by assuming the atmospheric pressure in Boulder, Colorado to be 0.85×101 Pa. (ii) As 1 mol of $NaBH_4$ produces 4 mol of H_2, the conversion factor for $[NaBH_4]$ into L of H_2 (NTP) was $V_{H_2} = 4(M_{NaBH_4} V_{solution} RT)/P$ using T (temperature) and P (pressure) as the corresponding values for NTP conditions. (iii) The 1 L of H_2 (NTP) generated in 1 min is equivalent to 100 W of electrical power at 0.7 V. (iv) The experiments were done with 4.7 mg of catalyst which contained 0.42 wt.% of Pt and 0.98 wt.% of Pd. The atomic weight of Pt and Pd are 195 and 106 g mol^{-1}. Thus, the catalyst used in the experiments contained 5×10^{-7} mol of metal atoms.

References

[1] L. Schlapbach, A. Züttel, Nature 414 (6861) (2001) 353–358.
[2] S.C. Amendola, S.L. Sharp-Goldman, M.S. Janjua, N.C. Spencer, M.T. Kelly, P.J. Petillo, M. Binder, J. Power Sources 85 (2) (2000) 186–189.
[3] K. Cowey, K.J. Green, G.O. Mepsted, R. Reeve, Curr. Opn. Solid State Mater. Sci. 8 (5) (2004) 367–371.
[4] Y. Kojima, K.-I. Suzuki, K. Fukumoto, Y. Kawai, M. Kimbara, H. Nakanishi, S. Matsumoto, J. Power Sources 125 (1) (2004) 22–26.
[5] H. Tsuchiya, O. Kobayashi, Int. J. Hydrogen Energy 29 (10) (2004) 985–990.
[6] J.-H. Wee, J. Power Sources 155 (2) (2006) 329–339.
[7] H.I. Schlesinger, H.C. Brown, A.E. Finholt, J.R. Gilbreath, H.R. Hoekstra, E.K. Hyde, J. Am. Chem. Soc. 7 (1) (1953) 215–219.
[8] B.D. James, M.G.H. Wallbridge, Prog. Inorg. Chem. 11 (1970) 200–231.
[9] Y. Kojima, K.-I. Suzuki, K. Fukumoto, M. Sasaki, T. Yamamoto, Y. Kawai, H. Hayashi, Int. J. Hydrogen Energy 27 (10) (2002) 1029–1034.
[10] Y. Kojima, K.-I. Suzuki, Y. Kawai, J. Power Sources 155 (2) (2006) 325–328.
[11] P. Krishnan, T.-H. Yang, W.-Y. Lee, C.-S. Kim, J. Power Sources 143 (1–2) (2005) 17–23.
[12] S. Ozkar, M. Zahmakiran, J. Alloys Compd. 404–406 (2005) 728–731.
[13] C. Wu, F. Wu, T. Bai, B. Yi, H. Zhang, Mater. Lett. 59 (14–15) (2005) 1748–1751.
[14] J.-H. Wee, K.-Y. Lee, S.H. Kim, Fuel Process. Technol. 87 (9) (2006) 811–819.
[15] M. Boudard, Adv. Catal. 20 (1969) 153–166.
[16] H.C. Brown, C.A. Brown, J. Am. Chem. Soc. 84 (35) (1962) 1493–1494.
[17] S.C. Amendola, M. Binder, M.T. Kelly, P.J. Petillo, S.L. Sharp-Goldman, Hydrogen Energy, Kluwer Academic/Plenun Press, New York, 2002, p. 69.
[18] S.C. Amendola, S.L. Sharp-Goldman, M.S. Janjua, N.C. Spencer, M.T. Kelly, P.J. Petillo, M. Binder, Int. J. Hydrogen Energy 25 (10) (2000) 969–975.
[19] S. Suda, Y.M. Sun, B.H. Liu, Y. Zhow, S. Morimitsu, K. Arai, N. Tsukamoto, M. Uchida, Y. Candra, Z.P. Li, Appl. Phys. A 72 (2) (2001) 209–212.
[20] C. Wu, H. Zhang, B. Yi, Catal. Today 93–95 (2004) 477–483.
[21] R. Raj, M.F. Ashby, Acta Metall. 23 (1975) 653–666.
[22] S.R. Shah, R. Raj, J. Eur. Ceram. Soc. 25 (2–3) (2005) 243–249.
[23] H.-Y. Ryu, R. Raj, J. Am. Ceram. Soc. (2006) (early on-line).
[24] S. O'Brien, M. Fishwick, B. McDermott, M.G.H. Wallbridge, G.A. Wright, Inorg. Synth. 13 (1971) 73–79.
[25] J.E. Gozum, D.M. Pollina, J.A. Jensen, G.S. Girolami, J. Am. Chem. Soc. 100 (1988) 2688–2689.
[26] E.J. Gozum, D.M. Pollina, J.A. Jensen, G.S. Girolami, J. Am. Chem. Soc. 110 (8) (1988) 2688–2689.
[27] A. Ansón, E. Lafuente, E. Urriolabeitia, R. Navarro, A.M. Benito, W.K. Maser, M.T. Martínez, Phys. Chem. B 110 (13) (2006) 6643–6648.
[28] T. Wang, X. Hu, X. Qu, S. Dong, J. Phys. Chem. B 110 (13) (2006) 6631–6636.
[29] Z.Q. Tian, S.P. Jiang, Y.M. Liang, P.K. Shen, J. Phys. Chem. B 110 (11) (2006) 5343–5350.
[30] Z.Q. Tian, F.Y. Xie, P.K. Shen, J. Mater. Sci. 39 (2004) 1507–1509.
[31] C.H. Yen, X. Cui, H.B. Pan, S. Wang, Y. Lin, C.M. Wai, J. Nanosci. Nanotechnol. 5 (2005) 1852–1857.
[32] T.W. Ebbesen, P.M. Ajayan, Nature 358 (6388) (1992) 220.
[33] S.J. Gregg, K.S.W. Sing, Adsorption, Surface Area and Porosity, Academic Press, London, 1982, pp. 285–286.
[34] E.P. Barret, L.G. Joyner, P.H. Halenda, J. Am. Chem. Soc. 73 (1) (1951) 373–380.

[35] A.S.C. Chan, J. Halpern, J. Am. Chem. Soc. 102 (1980) 838.
[36] K.A. Holbrook, P.J. Twist, J. Chem. Soc. A: Inorg. Phys. Theor. 7 (1971) 890–894.
[37] J.S. Zhang, W.N. Delgass, T.S. Fisher, J.P. Gore, J. Power Sources 164 (2007) 772.
[38] S.C. Amendola, S.L. Sharp-Goldman, M.S. Janjua, M.T. Kelly, P.J. Petillo, M. Binder, J. Power Sources 85 (2) (2000) 186–189.
[39] D. Hua, Y. Hanxi, A. Sinping, C. Chuansin, Int. J. Hydrogen Energy 28 (10) (2003) 1095–1100.